Dependence of Initial Cluster Aggregation Kinetics on Shear Rate for Particles of Different Sizes Under Turbulence

Lyonel Ehrl, Miroslav Soos, and Massimo Morbidelli
Institute for Chemical and Bioengineering, Dept. of Chemistry and Applied Biosciences, ETH Zurich, 8093 Zurich, Switzerland

Matthäus Ulrich Bäbler
Institute of Process Engineering, Dept. of Mechanical and Process Engineering, ETH Zurich, 8093 Zurich, Switzerland

DOI 10.1002/aic.11923
Published online August 11, 2009 in Wiley InterScience (www.interscience.wiley.com).

Initial aggregation kinetics for three particle sizes and broad range of Péclet numbers were investigated under turbulent conditions in stirred tank. This allowed us to observe the transition from diffusion-controlled to purely shear-induced aggregation. The evolution of the root-mean-square radius of gyration, zero-angle intensity of scattered light, and obscuration was obtained by small-angle static light scattering. For a given particle size the measured evolution of all integral quantities obtained for various volume average shear rates $\langle G \rangle$*, scales with a dimensionless time,* $\tau_{exp} = \alpha_{exp} \times \langle G \rangle \times \phi \times t$*. The experimentally obtained aggregation efficiency* α_{exp}*, follows the power law* $\alpha_{exp} = \mathrm{Pe}^{-n}$*, where* Pe *is the primary particle Péclet number. With increasing particle size a decrease in n is observed in accordance with theory and literature data. As previously predicted by population balance equation simulations three aggregation regimes were observed experimentally.* © 2009 American Institute of Chemical Engineers *AIChE J,* 55: 3076–3087, 2009

Keywords: aggregation efficiency, ortho-kinetic, peri-kinetic, hydrodynamic interactions, obscuration, turbidity, extinction

Introduction

Shear-induced coagulation is commonly used to separate fine solids from destabilized colloidal suspensions in wastewater treatment[1] or in the polymer industry, e.g., when dealing with latexes produced by emulsion polymerization.[2] Besides this, coagulation is often present as an undesired process when unstable dispersions of nano- or submicron-sized particles are processed. In such processes, assuming that density differences between the particles and the fluid are negligible, aggregation of primary particles to form clusters is the result of two distinct mechanisms, i.e., Brownian motion of the particles and velocity gradients within the suspending fluid (shear rate). The effect of Brownian motion on aggregation processes for attractive (diffusion-limited) and repulsive (reaction-limited) systems is well understood.[3–5] However, shear-induced aggregation, especially under turbulent conditions, is an ongoing issue for discussion in the literature.[6–17] One can estimate which mechanism prevails by means of the Péclet number of the particles (or aggregates) defined as the ratio of the time scale of diffusive

Additional Supporting Information may be found in the online version of this article.

Correspondence concerning this article should be addressed to M. Morbidelli at massimo.morbidelli@chem.ethz.ch

transport over the time scale of convective transport due to shear. As we consider the collision of two particles (or aggregates) for the diffusive transport D, the double of the single particle diffusion coefficient is used.[18] Thus

$$\mathrm{Pe} = \frac{Gr^2}{D} = \frac{3\pi\eta G r^3}{k_B T} \quad (1)$$

where η is the dynamic viscosity, G is the shear rate, r is the characteristic length-scale (particle radius or aggregate radius), k_B is the Boltzmann constant, and T is the absolute temperature.

In 1917 von Smoluchowski[19] proposed rate functions for both mechanisms, Brownian motion (perikinetic) and simple shear (orthokinetic), neglecting hydrodynamic interactions between the particles and the fluid or the particles themselves (rectilinear approach). This results in the rate of doublet formation being linearly proportional to the shear rate. For turbulent conditions Camp and Stein[20] and Saffman and Turner[21] applied the rectilinear approach assuming the shear rate to be proportional to the square root of the rate of turbulent energy dissipation. The introduction of functional forms for the aggregation rate under various conditions by such *ad hoc* models was a significant step into the direction of a successful modeling of these processes. Nevertheless, due to the linear dependency of the aggregation rate on the shear rate these models significantly overestimate the available experimental data.[9,22-27]

Half a century after von Smoluchowski, Spielman[28] and Honig et al.[29] independently evaluated the effect of hydrodynamic interactions to the rectilinear rate function for Brownian aggregation that occur when viscous interactions between two spheres are included, resulting in corresponding correction factors, which where later used to explain the experimental observations.[18]

In analogy to this in 1977 van de Ven and Mason[30] and Zeichner and Schowalter[31] independently evaluated the effect of hydrodynamic interactions for the aggregation rate function of similar-sized impermeable spheres in simple shear and elongational laminar flow using trajectory analysis. In their work the deviations from the rectilinear approach are expressed in the form of a prefactor, the so-called aggregation efficiency, which exhibits an inverse nonlinear proportionality with the shear rate of the flow. This theoretical work was then confirmed by the subsequent experimental work of Zeichner and Schowalter[32] for simple shear flow. A theoretical extension of the trajectory analysis to non-equal-sized impermeable spheres was presented by Adler[33,34] and Higashitani et al.[35] In these studies the contribution of Brownian motion to the aggregation phenomena was neglected, and therefore, their results are valid only for large Pélect number. However, for the first time the significance of hydrodynamic interactions, which are repulsive in nature, with respect to the van der Waals attraction was taken into account by introducing a dimensionless group $N_f = A_H/\eta G r^3$, which allows for the comparison of systems involving different materials, characterized by their Hamaker constant A_H.

With respect to the dimensionless groups defined up to this point we want to note the following. Relating the three contributing terms arising from Brownian motion, shear convection, and fluxes due to van der Waals attraction it is necessary to define two dimensionless groups representing the governing terms in the convection diffusion equation[18] and population balance equations.[17] Commonly one of the following two pairs of dimensionless groups, Pe and N_f or Pe and A_H/k_BT, is used. Usually, in shear aggregation for a given colloidal system at given temperature A_H, k_BT, and r_p (primary particle radius) are fixed, and G remains the only adjustable parameter. For practical reasons we will, therefore, consider the process of aggregation from the perspective of Pe and A_H/k_BT. As A_H/k_BT is constant for the systems investigated in this work our analysis will focus on the process dependency on Pe.

In contrast to trajectory analysis under laminar conditions Brunk et al.[36,37] took an approach that includes interparticle potentials to model doublet formation under turbulent conditions. The resulting aggregation rate constant is smaller than that predicted by Saffman and Turner[21] with an inverse nonlinear proportionality of the aggregation efficiency on the shear rate similar to the laminar flow cases.[30,31] In their subsequent work Brunk et al.[9] confirmed these theoretical predictions experimentally.

Up to this point, in the abovementioned literature on shear aggregation the aggregation event is considered to be adequately described by the collison of solid spheres. Strictly, this is only valid in the case of doublet formation, i.e., in the phase of initial aggregation. Due to the usually small size of primary particles this phase is dominated by Brownian motion and can be properly described by applying the expression provided by Spielman[28] and Honig et al.[29] However, as aggregation proceeds clusters of distinct structure are formed, whose hydrodynamic properties are different to those of solid spheres. Furthermore, as the aggregates grow their characteristic size rapidly exceeds the size range where Brownian motion is effective, i.e., the aggregate Péclet number increases indicating shear-induced aggregation to be the dominant mechanism. Consequently, in order to fully model real aggregation processes beyond doublet formation, one has to consider shear-induced aggregation events between clusters of different sizes and distinct structure.

To that effect, Kusters et al.[8] and Torres et al.[6] independently proposed models for the collision efficiency between clusters depicting aggregates as consisting of an impermeable core determining the hydrodynamics upon approach (and with it the trajectory lines for two colliding aggregates), and a completely permeable shell defining the collision radius. In contrary, Veerapaneni and Wiesner[7] considered that the aggregation efficiency can be modeled by the fluid collection efficiency calculated for single porous aggregates, neglecting the hydrodynamic interactions present between the approaching aggregates. As pointed out by Bäbler[17] all those models rely on strong assumptions regarding both hydrodynamic interactions and interparticle forces, as well as the aggregate permeability. Based on his trajectory analysis of colliding permeable spheres[14] Bäbler developed a collision efficiency model for flow-induced coagulation of fractal aggregates in the viscous subrange,[17] which was successfully applied by Bäbler et al.[16] to predict the regrowth kinetics of fully grown aggregates. However, these studies[14,16,17] focused mainly on the effects of hydrodynamic interactions on aggregation without emphasizing the effect of Brownian motion.

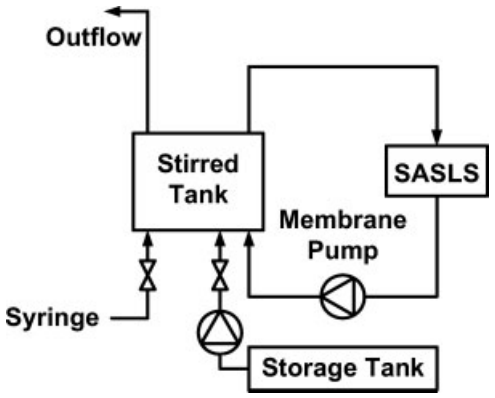

Figure 1. Schematic drawing of the experimental setup.

Therefore, the goal of this work is to provide experimental data of initial cluster aggregation kinetics for different primary particle diameters to cover the transition from diffusion-controlled aggregation to purely shear-induced aggregation and present its scaling with shear rate. To our knowledge, there exists only one comparable work on this topic in literature, i.e., Selomulya et al.,[12] but due to the experimental procedure and the low resolution of the initial cluster aggregation kinetics for the smaller primary particles, their data cannot be used to study the aforementioned transition. By comparing the evolution of measured integral quantities with simulation data[15] three distinct regimes of aggregation could be identified, i.e., diffusion-controlled, transition, and purely shear-induced aggregation. Since Soos et al.[38] found that the scaling of the initial aggregation kinetics with shear rate holds not only for doublet formation but also beyond this limit, the scaling results for the initial cluster aggregation kinetics of this work will be compared with those of pure doublet formation presented in the literature.

Materials, Methodology, and Measurement Method

Materials and methodology

In the experiments two white sulfate polystyrene latexes were used, both supplied by Interfacial Dynamics Corporation (Portland, OR, USA) (product-no: 1-400, coefficient of variation = 4.0%, batch no: 1034,2, solid% = 8.0, surface charge density: 48 mC/m^2; product-no: 1-00, coefficient of variation = 8.4%, batch no: 1614,1, solid% = 4.1, surface charge density: 67 mC/m^2). The mean diameter of the latex particles were equal to 420 nm and 120 nm, as measured by small-angle static light scattering (SASLS), in agreement with the particle size declared by the producer. The measured particle-size distributions were very narrow. Hence, the latexes can be considered as monodisperse. The latexes were chosen so as to ensure similar surface chemistry (nature and number of surface charge groups per surface area) to the latex with primary particles size equal to 810 nm used in our previous work.[38] Hence, the primary particle diameter is the only changing parameter and, therefore, its effect can be studied independently from other phenomena that might be induced by a variation in the surface or bulk chemistry of the particles.[39]

All experiments were performed in a 2.5 L stirred-tank coagulator shown schematically in Figure 1 (diameter: 150 mm, height: 150 mm, baffled with 4 cylindrical bars with a diameter of 12 mm mounted off-wall at 55 mm from the center, impeller: Rushton turbine with a diameter of 60 mm placed 50 mm from the bottom, sampling ports: located at the bottom, 40 mm from center, power number obtained from CFD simulations: 2.74; further details can be found in Waldner et al.[13]). The tank was operated at stirring speeds ranging from 200 to 1,073 rpm.

The initial suspension of primary particles with a solid volume fraction ϕ, equal to 1×10^{-5} or 2×10^{-5} was prepared by diluting the original latex with an appropriate amount of deionized water. Subsequently, the diluted latex was pumped from a storage tank into the coagulator. An overflow tube was used as a small reservoir of about 100 mL in order to allow replenishing of the coagulator with liquid during sampling and to prevent air from entering the coagulator (see Figure 1). The aggregation process was started by adding a coagulant solution (30 mL of 20% (w/w) $Al(NO_3)_3$ in water). The resulting salt concentration was well above the critical coagulation concentration for the given system, i.e., the electrostatic repulsive forces between the particles were fully screened and the particles were completely destabilized. In order to achieve a good reproducibility of the initial aggregation kinetics a programmable syringe pump, *Vit-Fit* (Lambda, Czech Republic), was used for salt injection. The corresponding injection time was approximately 15 s. The typical mixing time of the injected salt solution is about 5 s at 200 rpm (tested by dye measurements),[40] which is at least one-order of magnitude below the characteristic time of aggregation at all conditions considered in this work, (cf. section Fluid Flow Characterization). The time evolution of the coagulating system was monitored through small-angle static light scattering (SASLS). For this, a sampling loop was installed that pumped the suspension from the tank to a measuring cell and back to the tank. The pump was thereby placed after the measuring cell. Aggregate breakage within the sampling loop was prevented by properly adjusting the flow rate in the sampling loop.[40] Aggregate breakage in the pump can be ignored due to the large volume of the tank with respect to the sampling loop. A list of all investigated process conditions can be found in Table 1. A discussion of the steady-state response of the systems properties on either a variation of the shear rate or on a variation of the solid-volume fraction can be found in our previous work.[41]

Small-angle static light scattering (SASLS)

A SASLS instrument, *Mastersizer 2000* (Malvern, U.K.), was used in all experiments for online characterization of the cluster mass distributions (CMD). In SASLS the intensity of scattered light is measured as a function of the scattering angle. The former can be expressed as[42]

$$I(q) = I(0)P(q)S(q) \tag{2}$$

where $I(0)$ is the zero-angle intensity of scattered light, $P(q)$ is the form factor (due to primary particles), and $S(q)$ is the

Table 1. List of Experimentally Investigated Process Conditions in This Work: d_p, Primary Particle Diameter; $\langle G \rangle$, Volume Average Shear Rate, ϕ, Solid Volume Fraction, Pe, Primary Particle Péclet Number; $A_H/k_BT = 3.33$ for All Experiments at Room Temperature, with a Hamaker Constant for Polystyrene $A_H = 1.37 \times 10^{-20}$ J[60]

label	d_p/(nm)	$\langle G \rangle$/(1/s)	Pe/(−)	ϕ/(−)	symbol used in Figure 2 to Figure 4
120-1	120	108	5.3×10^{-2}	1×10^{-5}	□
120-2		108	5.3×10^{-2}	2×10^{-5}	■
120-3		350	1.7×10^{-1}	1×10^{-5}	◁
120-4		959	4.7×10^{-1}	1×10^{-5}	●
120-5		1216	6.0×10^{-1}	2×10^{-5}	△
420-1	420	108	2.3×10^{0}	1×10^{-5}	□
420-2		108	2.3×10^{0}	2×10^{-5}	■
420-3		350	7.4×10^{0}	2×10^{-5}	◁
420-4		613	1.3×10^{1}	1×10^{-5}	○
420-5		613	1.3×10^{1}	2×10^{-5}	●
420-6		1216	2.6×10^{1}	2×10^{-5}	△
810-1	810	108	1.6×10^{1}	4×10^{-5}	○
810-2		325	4.9×10^{1}	4×10^{-5}	▲
810-3		613	9.3×10^{1}	4×10^{-5}	▽
810-4		959	1.5×10^{2}	4×10^{-5}	◆
810-5		1353	2.0×10^{2}	4×10^{-5}	□

The data for $d_p = 120$ and 420 nm was produced in this work, the data for $d_p = 810$ nm is taken from Soos et al.[38]

structure factor (due to the arrangement of primary particles within the aggregates). The scattering vector amplitude q, is defined as

$$q = 4\pi \frac{n}{\lambda} \sin\left(\theta/2\right) \tag{3}$$

where θ is the scattering angle, n is the refractive index of the dispersing fluid, and λ is the laser wavelength in vacuum. For the present system $n = 1.33$ (water) and $\lambda = 633$ nm.

Analysis of the measured scattered intensity in the Guinier region (for qR_g up to about unity) allows one to extract certain characteristic quantities of the CMD, namely the root-mean-square (rms) radius of gyration, $\langle R_g \rangle$, and the zero-angle intensity, $I(0)$. Detailed description of the evaluation of $\langle R_g \rangle$ and $I(0)$ can be found in our previous work.[38,40,41]

Within the limits of the RDG theory, i.e., when $|m - 1| \leq 1$ and $(4\pi r_p/\lambda)|m - 1| \leq 1$, where m is the relative refractive index of the latex particles with respect to the dispersant, $I(0)$ scales with the second power of the scatterer's mass and it constitutes the second-order moment of the CMD.[42–45] Outside these limits, i.e., for primary particles of a size comparable to or larger than the laser wavelength[46,47] or for dense aggregates where multiple light scattering within the aggregate takes place,[46,48] the latter is not anymore true. In this case the intensity of the forward scattered light scales with the mass of the scatterer to a power smaller than two. Accordingly, $I(0)$ will not anymore correspond to the second-order moment of the CMD but instead to a smaller moment.

SASLS further provides the obscuration of the measured dispersion, which corresponds to the total amount of light lost due to scattering and absorption by primary particles and aggregates. The obscuration Ob, is described by the Lambert-Beer's law as follows[49]

$$\ln(1 - Ob) = -\tau L = -NC_{ext}L \tag{4}$$

where τ is the turbidity, N is the number concentration of particles (aggregates) per unit volume, $C_{ext} = C_{sca} + C_{abs}$ is the total extinction cross section per aggregate, with C_{sca} and C_{abs} being the scattering cross section and the absorption cross section, respectively, and L is the path length that the light passes through the dispersion (2.4 mm in the present case). In the case of polystyrene particles, the light lost due to absorption is negligible and $C_{ext} = C_{sca}$. Relations for the total scattering cross section C_{sca}, are available for fractal aggregates consisting of RDG scatterers and absence of multiple scattering, i.e., open aggregaets.[42] For dense fractal aggregates that consist of non-RDG scatterers, as it is the case of this work[41] and for most aggregates formed under shear, no such relation exists.[50,51] Thus, a quantitative interpretation of obscuration data alone is not possible for the present system. However, comparison of obscuration data with the other two measured quantities allows us to draw conclusions regarding the extinction cross section, and hence, the characteristics of the aggregate size distribution.

Fluid flow characterization

It is known that within a stirring device the shear rate does not assume a unique value but it exhibits a distribution that is characteristic of the device. Nevertheless, it has become common to use the volume average shear rate $\langle G \rangle$, to characterize different process conditions and to calculate Pe or N_f. However, it has to be kept in mind that such a reduction to volume averaged quantities is only valid in cases were the timescale of aggregation is much larger than the time scale of mixing.[40] For fully destabilized systems this is only the case for very low solid-volume fractions.[52,53]

For present systems the time scale of mixing is in the order of a few seconds (approximately 5 s at 200 rpm, as tested by dye measurement). As the focus of this work lays on the initial aggregation kinetics the timescale of aggregation is estimated by the inverse of the doublet formation rate,[40] thus $\tau_A = (\alpha_A \langle G \rangle d_p^3 N)^{-1}$, where α_A is the aggregation efficiency, and N the number concentration of the primary particles. Using $N = \phi/V_p$, where V_p is the primary particle

volume, and $\alpha_A \approx 0.2$,[40] mentioned expression reduces to $\tau_A = \pi/(1.2\langle G\rangle\phi)$. Therefore, the time scale of aggregation is independent of the primary particle size and takes values in the range from 2500 s ($\langle G\rangle = 108\ s^{-1}$, $\phi = 1 \times 10^{-5}$) down to 100 s ($\langle G\rangle = 1{,}300\ s^{-1}$, $\phi = 2 \times 10^{-5}$). This is well above the mixing time justifying the use of the volume averaged shear rate to characterize the aggregation process.

In order to evaluate $\langle G\rangle$ we performed computational fluid dynamics simulations of the fluid flow in the coagulator using commercial software, Fluent version 6.2 from Ansys Inc. (Canonsburg, PA, USA). To model turbulence in the simulations a standard k-ε model was applied. From the local values of the energy dissipation rate ε, one can calculate local values of the shear rate according to $G = \sqrt{\varepsilon/\nu}$ which then can be averaged over the vessel volume to obtain $\langle G\rangle$. For more details on the computational fluid dynamics simulation we refer to the work of Soos et al.[38,54]

Results and Discussion

In the following discussion we will focus on the initial cluster aggregation kinetics of destabilized suspensions of primary particles with varying diameter (120 nm, 420 nm, and 810 nm), and its scaling behavior with respect to the volume average shear rate. Various integral quantities of the CMD, i.e., averaged aggregate sizes, serve as a basis for the discussion. The integral quantities are extracted from intensity curves of scattered light as a function of the scattering wave vector amplitude, $I(q)$. The latter is obtained by in-loop SASLS measurements and the extracted integral quantities are $\langle R_g\rangle$, $I(0)$, and Ob. By dividing these quantities by the corresponding values at $t = 0$ one obtains normalized quantities $\langle R_g\rangle_n = \langle R_g\rangle/R_{g,p}$, $I(0)_n = I(0)/I(0)_{t=0}$, and $Ob_n = Ob/Ob_{t=0}$. Further, in order to follow the evolution of the polydispersity of the CMD we use the ratio between the first two integral quantities, defined as $M = I(0)_n/\langle R_g\rangle_n$.[15]

Effect of Brownian and shear aggregation on initial aggregation kinetics

The latexes used in our study exhibit a significant variation of the primary particle size. Thus, we expect to observe different regimes of aggregation, i.e., diffusion-controlled aggregation for the smaller particles and purely shear-induced aggregation for the larger particles. Evaluating the primary particle Péclet number using Eq. 1 with $T = 298$ K and $\langle G\rangle$ ranging from 108 s^{-1} to 1,353 s^{-1} we find Pe ranging from 1.7×10^1 to 2.0×10^2, from 2.2×10^0 to 2.9×10^1, and from 5.3×10^{-2} to 6.0×10^{-1} for primary particle diameters equal to 810 nm, 420 nm, and 120 nm, respectively (cf. Table 1). This suggests that for the larger primary particles (810 nm, 420 nm) shear dominates the initial aggregation process over the entire range of shear rates applied, whereas for the smaller primary particles (120 nm) Brownian motion governs the initial aggregation. However, due to the cubic dependence of Pe on the aggregate radius r (cf. Eq. 1) Pe rapidly increases with increasing aggregate size, and already for aggregates made up of a few primary particles we have Pe $\gg$ 1 even in the case of 120 nm primary particles. Hence, shear aggregation becomes dominant even in this case.

In order to understand the interplay between Brownian and shear aggregation, in Figure 2 we show the initial aggregation kinetics as a function of the dimensionless time for shear aggregation, $\tau_s = \langle G\rangle \times \phi \times t$. The dashed lines serve to distinguish the shape of the time evolution of the measured integral quantities whereas the solid lines serve to guide the eye. The time evolution of both measured integral quantities (i.e., $\langle R_g\rangle_n$ and $I(0)_n$) for a given primary particle size are very similar. However, they are substantially different for different primary particle size. In particular, we observe a concave evolution for $d_p = 120$ nm (Figure 2a, d), an exponential growth for $d_p = 420$ nm (Figure 2b, e), and a convex evolution for $d_p = 810$ nm (Figure 2c, f). Considering further the moment ratio M, we observe a monotonic increase for $d_p = 120$ nm (Figure 2g), an approximately constant value for $\tau_s < 0.4$ followed by a monotonic increase for $d_p = 420$ nm (Figure 2h), and a monotonic decrease for $d_p = 810$ nm (Figure 2i). To our best knowledge this is the first time that the transition from aggregation dominated by Brownian motion (concave growth, increasing M) to clearly flow-induced aggregation (convex growth, decaying M) is shown experimentally by measuring kinetics of higher order integral quantities. Previously, such a change in the shape of the time evolution of the CMDs integral quantities was observed only in simulations.[15]

For the interpretation of the experimental observations described earlier one need's to consider the derivation of the integral quantities from the CMD and the relation between the individual integral quantities themselves. First, $I(0)_n$ is obtained by a lower weighting of the aggregate mass than $\langle R_g\rangle_n$ and, as a result, $I(0)_n$ characterizes aggregates of smaller size than $\langle R_g\rangle_n$. Second, it was shown experimentally by Ehrl et al.[41] and theoretically by Lattuada et al.[51] that for self-similar CMDs these two quantities can be related according to a power law, $I(0)_n \propto \langle R_g\rangle_n^{d_f(1-c)}$. Here, d_f is the mass fractal dimension and c is a light scattering parameter, which accounts for deviations from the RDG theory, with $d_f\ (1 - c)$ being always larger than unity. These two characteristics suffice to interpret the observed evolution of the moment ratio M. In the case of a CMD with constant polydispersity and increasing average size (that is a form of self-similarity) the relation given earlier suggests that M increases with time. On the other hand, for a broadening CMD the different weighting of $I(0)_n$ and $\langle R_g\rangle_n$ leads to a decrease of M since $\langle R_g\rangle_n$ (largest aggregates) evolves faster than $I(0)_n$ (mass average aggregates).

For the case of Pe $\ll$ 1 (small primary particles) the initial aggregation kinetics is dominated by Brownian aggregation where due to preferential aggregation between large and small clusters the resulting CMD is rather narrow with a decreasing polydispersity. That is, the CMD is expected to be similar to the one produced through diffusion-limited cluster aggregation under static conditions.[55] Hence, the moment ratio is expected to monotonically increase as indeed is observed in Figure 2g. On the other hand, for Pe $\gg$ 1 the aggregation kinetics is dominated by shear where the cubic dependency of the aggregation rate on the aggregate size favors aggregation events between large aggregates. This leads to a broadening of the CMD with time and, consequently, results in a decay of M as it is indeed observed in (Figure 2i). Finally, at a Péclet number

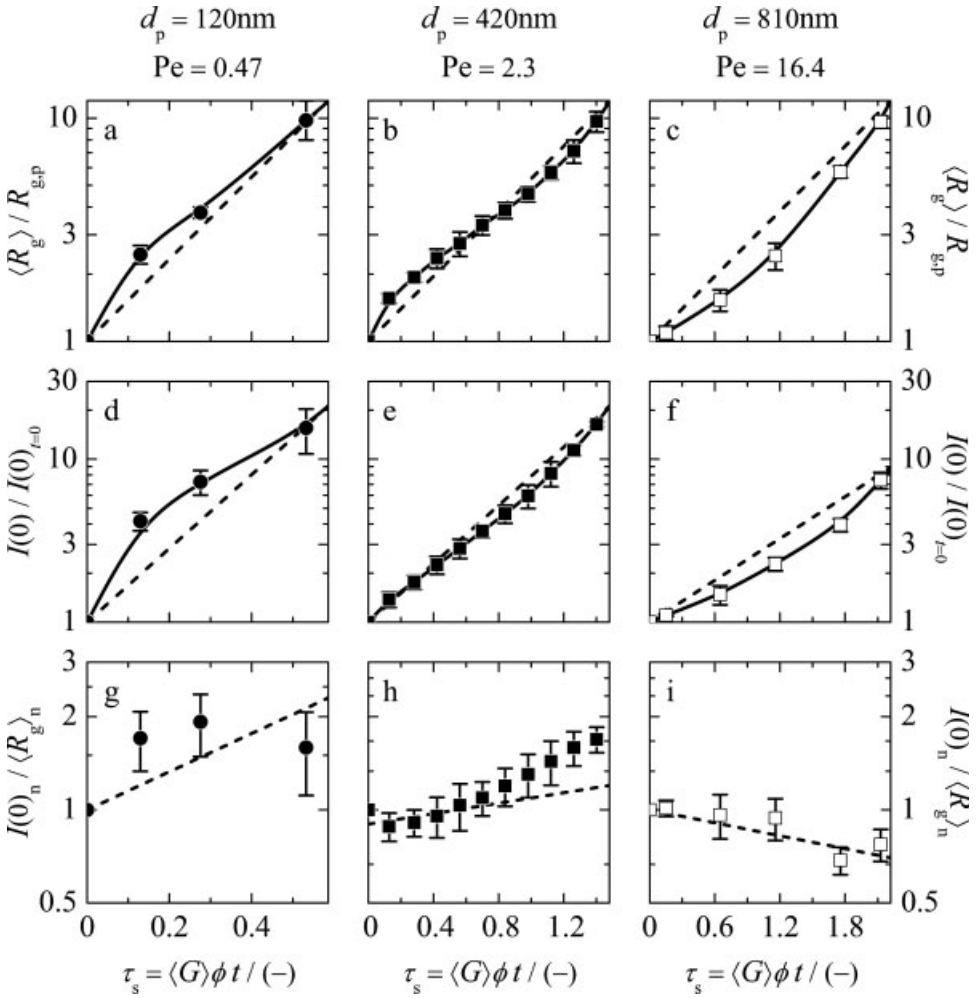

Figure 2. Evolution of (a,b,c) the normalized rms radius of gyration, $\langle R_g \rangle_n = \langle R_g \rangle / R_{g,p}$, (d,e,f) the normalized zero-angle intensity, $I(0)_n = I(0)/I(0)_{t=0}$, and (g,h,i) their ratio $M = I(0)_n / \langle R_g \rangle_n$ as a function of $\tau_s = \langle G \rangle \times \phi \times t$ for d_p equal to (a,d,g) 120 nm with Pe = 0.47, (b,e,h) 420 nm with Pe = 2.3, and (c,f,i) 810 nm with Pe = 16.4 up to a value of $\langle R_g \rangle_n$ around 10.

The dash-dotted lines serve to distinguish the shape of the time evolution of the integral quantities and the thick lines only serve to guide the eyes.

around unity shear aggregation becomes equally important than Brownian aggregation. In this case, the broadening of the CMD and the increase of the average cluster size act in a different way on the moment ratio M, and under proper conditions they can even balance each other. Such a situation is observed for $d_p = 420$ nm where M remains approximately constant over the very initial part of the aggregation process ($\tau_s < 0.4$), as shown in Figure 2h.

It is worth pointing out that similar observations were obtained using a population balance model to study the interplay between Brownian and shear aggregation.[15] From these simulations it is further deduced that for Pe $\rightarrow \infty$ a decrease in M is only possible when $d_f < 2$ (the value $d_f = 2$ is, however, only generic for the population balance model studied by Soos et al.[15] that neglects hydrodynamic and colloidal interactions of the particles, accounting for these interactions a decrease in M is also found for slightly larger d_f.[17] Moreover, for Pe $\rightarrow$ 0 where the process is controlled by Brownian aggregation values of d_f around 1.8 are expected as measured under static conditions.[4] From these two limits, we conclude that under any condition the initial clusters are rather open with $d_f < 2$, and only a weak dependency of the aggregation mechanism on the aggregate structure is expected. This is in agreement with a previous study in a laminar flow where both shear and Brownian aggregation were present.[6] The different shapes of the time evolution of the integral quantities are solely caused by the variation of the relative importance of Brownian aggregation with respect to shear aggregation on the growth and broadening of the CMD.

Shear aggregation until steady state for various shear rates and primary particle sizes

Soon after the initial part of the aggregation process, which is both affected by Brownian and shear aggregation the aggregates grow to sizes where the aggregate Péclet number, i.e., Eq. 1 with $\langle R_g \rangle$ substituting for r, becomes significantly larger than unity. At this stage, Brownian

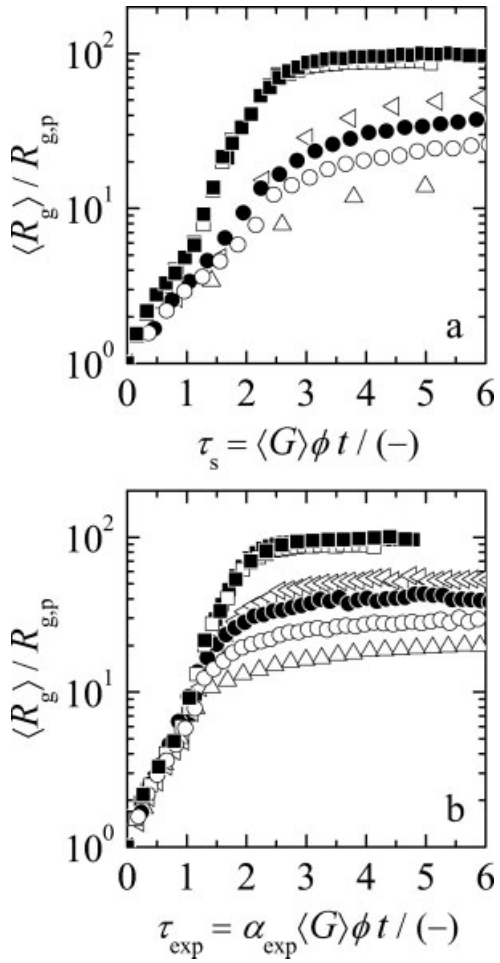

Figure 3. Evolution of the normalized rms radius of gyration, $\langle R_g \rangle_n = \langle R_g \rangle / R_{g,p}$, as a function of (a) $\tau_s = \langle G \rangle \times \phi \times t$, and (b) $\tau_{exp} = \alpha_{exp} \times \langle G \rangle \times \phi \times t$ for d_p = 420 nm with Pe = [2.2×10^0, 2.9×10^1].

aggregation becomes negligible and the process is dominated by shear aggregation which results in a self-accelerating kinetics expressed through an exponential aggregate growth. After having reached a certain size aggregate breakup sets in causing the growth rate to relax until eventually the CMD reaches a steady state. An example of the evolution of the aggregate size $\langle R_g \rangle_n$, as a function of $\tau_s = \langle G \rangle \times \phi \times t$ for various values of $\langle G \rangle$ and $d_p = 420$ nm is presented in Figure 3a. The steady-state values depend on the stirring speed and they are decreasing with increasing $\langle G \rangle$.[41] Furthermore, there is a small though significant difference in the evolution of $\langle R_g \rangle_n$ for different stirring speeds even when plotted vs. a dimensionless time τ_s. This latter finding has two reasons. First, the aggregation efficiency $\alpha_{i,j}$, which is a complex function of the masses i and j of the colliding aggregates and the aggregate structure, depends nonlinearly on the shear rate.[17,30,31] Hence, normalizing the time with $\langle G \rangle$ as done in Figure 3a still allows for distinguishing between experiments run at different $\langle G \rangle$. Second, the CMD, whose evolution at this stage of the process is controlled by shear, remembers its early stages where Brownian aggregation was important.

To account for these two nonlinear phenomena, here, we introduce an effective dimensionless time[38] $\tau_{exp} = \alpha_{exp} \times \langle G \rangle \times \phi \times t$ where $\alpha_{exp} = Pe^{-n}$ is a scaling factor that depends on Pe with n being a real number in the range from 0 to 1 representing pure shear-induced and Brownian aggregation, respectively. A rational for such a scaling relation is given by Bäbler[17] who studied aggregation under shear in the limit $Pe \rightarrow \infty$ by means of a population balance model that uses a detailed aggregation efficiency model.[17] It was found that in a limited range of N_f the evolution of the CMD can be described through a uniform aggregation efficiency $\alpha_c = f(N_f) = f(Pe, A_H/k_BT)$, i.e., an aggregation efficiency which is constant with respect to aggregate mass. Such an uniform aggregation efficiency can be factored out of the population balance equation leading to a dimensionless time of the form given above. Similar findings are made in the theoretical works of van de Ven[30,56,57] and Adler,[33,34] and in experimental studies[9,22–25] on doublet formation under shear.

Hereafter, the scaling exponent n is chosen such that for a given primary particle size are the initial cluster aggregation kinetics measured at different $\langle G \rangle$ fall on top of each other when plotted vs. τ_{exp}. The result of such a rescaling for the evolution of $\langle R_g \rangle_n$ as a function of τ_{exp} for various values of $\langle G \rangle$ and $d_p = 420$ nm is shown in Figure 3b where for this primary particle size a scaling exponent of $n = 0.25$ was found.

To validate the generality of this approach it was applied to all measured integral quantities, i.e., $\langle R_g \rangle_n$, $I(0)_n$, Ob_n, and M, as well as to different primary particle sizes. The rescaled time evolution of all these quantities is presented in Figure 4. It can be seen that for each primary particle size there exists a value of n such that the evolution of all three measured integral quantities fall on top of each other at least for $\tau_{exp} < \tau^*_{exp}$, where τ^*_{exp} is equal to 2, 1.25, and 1 for d_p equal to 120 nm, 420 nm, and 810 nm, respectively. The corresponding values of n for each primary particle size are equal to 0.6, 0.25, and 0.18, respectively.

Furthermore, in our previous work[41] where we used the same lattices we found that at steady state the aggregate structure is very compact, with $d_f = 2.64 \pm 0.18$. Hence, there is a substantial change in the aggregate structure[58,59] evolving from $d_f < 2$ in the initial stage of the process up to $d_f \approx 2.6$ at steady state. However, measuring this process of restructuring is difficult. The main reasons for this are the small relative aggregate size, the polydispersity of CMDs obtained at later stages of pure shear aggregation, and the fragility of open aggregates. The former two impede a well developed power-law region of an online measured structure factor, which complicates the determination of d_f from light scattering data. The latter make off-line microscopic investigations difficult as sampling usually leads to aggregate breakup or structural changes.

Evolution of obscuration

The evolution of the normalized obscuration for all three primary particle sizes is shown in Figure 4c, g, and k, respectively. For the small particles ($d_p = 120$ nm, Figure 4c) Ob_n exhibits a similar behavior as the other measured integral quantities. That is, it increases monotonically with time until it reaches steady state at the same time as $\langle R_g \rangle_n$ and $I(0)_n$. This trend is in agreement with RDG theory which

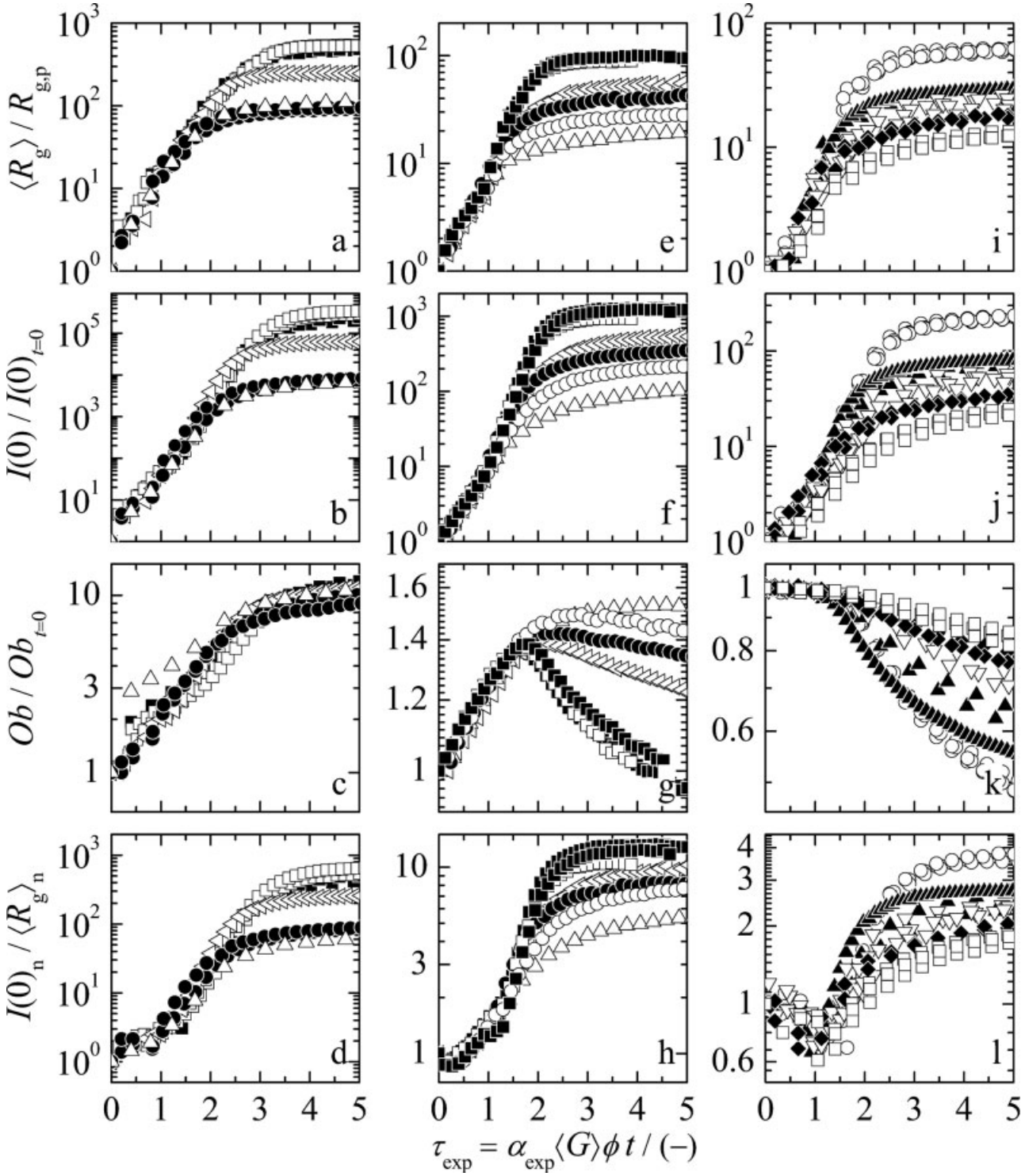

Figure 4. Evolution of (a,e,i) the normalized rms radius of gyration, $\langle R_g \rangle_n = \langle R_g \rangle / R_{g,p}$, (b,f,j) the normalized zero-angle intensity, $I(0)_n = I(0)/I(0)_{t=0}$, (c,g,k) the normalized obscuration, $Ob_n = Ob/Ob_{t=0}$, and (d,h,l) the moment ratio, $M = I(0)_n/\langle R_g \rangle_n$ as a function of $\tau_{exp} = \alpha_{exp} \times \langle G \rangle \times \phi \times t$ for d_p equal to (a–d) 120 nm, $\alpha_{exp} = Pe^{-0.6}$, (e–h) 420 nm, $\alpha_{exp} = Pe^{-0.25}$, and (i-l) 810 nm, $\alpha_{exp} = Pe^{-0.18}$.

predicts an extinction cross section of a single aggregate that is proportional to the square of the aggregates mass.[42–45] For a system of constant solid volume fraction and variable aggregate size this results in an obscuration of the population that scales linearly with the average aggregate mass.[41]

For the intermediate particles (d_p = 420 nm, Figure 4g) the particle size approaches the wave length of the laser of the light scattering device (λ = 633 nm) and, therefore, the RDG approximation is not anymore appropriate. This is reflected in the distinct evolution of the obscuration for this

Table 2. Values of the Exponent n for the Power-Law Scaling Between Aggregation Efficiency, α_{exp}, and the Primary Particle Péclet Number, Pe, (or Volume Average Shear Rate, $\langle G \rangle$, as All Other Parameters are Fixed for the Given Systems), for Systems with Different Primary Particle Sizes, d_p, and Hamaker Constants, A_H, Under Turbulent Conditions

Literature source	d_p/nm	$\langle G \rangle$/(1/s−)	Pe/(−)	n
Brunk et al.[9] [1,*]	3900	[3.7, 83.6]	$[6.3 \times 10^1, 1.4 \times 10^3]$	0.16
Higashitani et al.[23] (Fig. 10)[2,*]	850	[40, 280]	$[7.0 \times 10^0, 4.9 \times 10^1]$	0.24
Higashitani et al.[23] (Fig. 10)[2,*]	2170	[40, 280]	$[1.2 \times 10^2, 8.3 \times 10^2]$	0.21
Kobayashi et al.[25] (Fig. 7)[2,*]	1365	[18, 580]	$[1.3 \times 10^1, 4.1 \times 10^2]$	0.29
Birkner and Morgan[22] (Table 1)[2,*]	1030	[11, 120]	$[3.4 \times 10^0, 3.7 \times 10^1]$	0.18
De Boer and Hoedemaker[24] (Fig. 5)[2,*]	740	[150, 1200]	$[1.7 \times 10^1, 1.4 \times 10^2]$	0.28
Gruy[11] (Fig. 6)[3,†]	500	[26, 318]	$[9.3 \times 10^{-1}, 1.1 \times 10^1]$	0.4
Tontrup et al.[10] (Fig. 6a)[3,‡]	[350, 440]	[89, 502]	$[1.1 \times 10^0, 1.2 \times 10^1]$	0.38
Ehrl et al. (this work)[3,*]	120	[108, 1300]	$[5.3 \times 10^{-2}, 6.0 \times 10^{-1}]$	0.6
Ehrl et al. (this work)[3,*]	420	[108, 1300]	$[2.2 \times 10^0, 2.9 \times 10^1]$	0.25
Soos et al.[38] [3,*]	810	[108, 1376]	$[1.7 \times 10^1, 2.0 \times 10^2]$	0.18
Bäbler et al.[16] [3,*]	100	[108, 328]	$[3.1 \times 10^{-2}, 9.5 \times 10^{-2}]$	0.5
Bäbler et al.[16] [3,*]	600	[108, 1376]	$[6.7 \times 10^0, 8.5 \times 10^1]$	0.25
Moussa et al.[39] [3,*]	300	[108, 328]	$[8.3 \times 10^{-1}, 2.5 \times 10^0]$	0.38

[1] n is provided directly
[2] n was obtained by scaling the provided $\alpha_{doublet}$ and $\langle G \rangle$
[3] n was obtained by scaling the provided aggregation kinetic onto a single curve
*polystyrene - water, $A_H = 1.37 \times 10^{-20}$ J[60] and $A_H/k_BT = 3.33$
†fused silica – water, $A_H = 8.5 \times 10^{-21}$ J[18] and $A_H/k_BT = 2.06$
‡titania – water, $A_H = 6 \times 10^{-20}$ J[61] and $A_H/k_BT = 14.6$

d_p shown in Figure 4g. In the initial part of the process ($\tau_{exp} < 1.5$) an increase in Ob_n can be observed for all conditions, concomitant with $\langle R_g \rangle_n$ and $I(0)_n$, whereas for $\tau_{exp} > 1.5$ the curves start to fan out. Most strikingly, besides steady-state plateaus also decreasing evolutions can be observed. The curves with steady-state plateaus are thereby obtained for higher $\langle G \rangle$ and, accordingly, relate to lower $\langle R_g \rangle_n$ and $I(0)_n$, whereas the curves with decreasing evolution are obtained for lower $\langle G \rangle$ and relate to higher $\langle R_g \rangle_n$ and $I(0)_n$, respectively. This implies that the aggregate extinction cross section of large aggregates built of large primary particles deviates over-proportionally from that predicted by RDG theory such that the obscuration of a population of large aggregates (as found at low stirring speed) can even be lower than that of a population of small aggregates (as found at high-stirring speed). A similar finding is made for large solid particles where the specific turbidity τ/ϕ scales inversely with particle size.[43] The clear and sharp forking in the measurements at $\tau_{exp} \approx 1.5$ (Figure 4g) suggests further that the aforementioned deviation from RDG theory occurs sharply at a certain aggregate size; the measured obscuration is mainly due to aggregates below this critical size, whereas larger aggregates have only a small contribution. Accordingly, the slow decay of Ob_n at late times for low-stirring speeds is caused by a slow consumption of the small aggregates and primary particles.[17] Notably, the consumption of these small species takes longer than it takes for the large aggregates (measured through $\langle R_g \rangle_n$ and $I(0)_n$) to reach steady state. As a result Ob_n decreases even after $\langle R_g \rangle_n$ and $I(0)_n$ reached steady state, where the larger the steady-state aggregate size the steeper the decrease in Ob_n.

For the largest particles ($d_p = 810$ nm, Figure 4k) the characteristic length scale of the scatterer is always larger than the laser wave length and, therefore, the RDG approximation is clearly not applicable anymore. This becomes obvious from the evolution of the obscuration with dimensionless time shown in Figure 4k. At the very initial part of the process ($\tau_{exp} < 1$) a very slow decay of the obscuration is observed. At this stage of the process the effects of aggregate growth and concomitant reduction of the aggregate number concentration nearly level out each other. For $\tau_{exp} > 1$ the increase of the extinction cross section with aggregate mass cannot anymore balance the reduction in the aggregate number concentration, and the obscuration of the population starts to decrease even stronger with aggregate size.

In summary, the evolution of the obscuration of a aggregate population ever deviates stronger from the RDG predictions as the primary particle size becomes comparable to or larger than the laser wavelength.[46,47,50] Furthermore, it is noted that for all primary particle sizes the aggregate structure at the end of the process is very compact,[41] which can lead to the additional effect of multiple light scattering within an aggregate.[46,48] From these findings it is obvious that the interpretation of turbidity data is a delicate task and it strongly depends on the scattering properties of the system. These are determined by the primary particle size (length scale of the smallest scatterer) with respect to the laser wave length, the aggregate size and structure, and, of course, the dielectric properties of the dispersed phase and the medium.

Comparison with experimental literature data

From the exponential growth phase of the observed cluster-cluster aggregation kinetics (Figure 4), we obtained $\alpha_{exp} \propto G^{-0.6}$ for Pe < 1, $\alpha_{exp} \propto G^{-0.25}$ for Pe ≈ 1, and $\alpha_{exp} \propto G^{-0.18}$ for Pe > 1. Such obtained values of the exponent n can be compared to the experimental doublet and cluster formation kinetics data obtained for various particle sizes and materials in different types of turbulent flows published in the literature.[9,16,22–25,38,39] A summary of the used operating conditions used in the literature data, characterized by d_p, $\langle G \rangle$, and the dimensionless groups Pe and A_H/k_BT, where

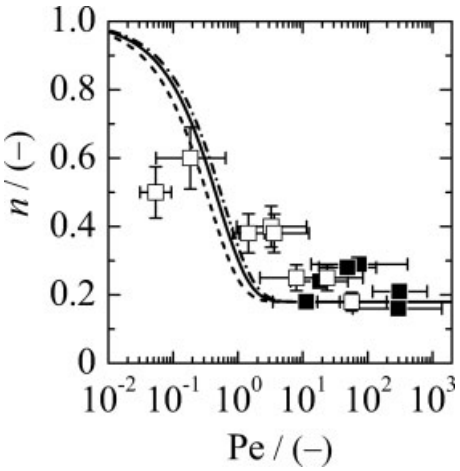

Figure 5. Exponent *n* vs. Pe: (■) from doublet formation rates,[9,22–25] (□) from aggregation kinetics.[10,11,16,38,39]

(The lines represents the solution of Eq. 9 of the Supporting Information for a Hamaker constants of (solid) polystyrene, (dashed) silica, and (dash-dotted) titania. Eq. 9 in Supporting Information is derived from a theoretical expression presented by Zaccone et al.[62] for the doublet formation rate due to both Brownian and shear-induced aggregation.)

the latter was calculated using Hamaker constants for polystyrene in water,[60] titania in water,[10] and for fused silica in water,[61] is presented in Table 2 and in Figure 5.

It can be seen that for large values of Pe the data scatters around the theoretically predicted value for doublet formation in the limit Pe $\rightarrow \infty$ that reads as $n = 0.18$.[30,31,33–35] For decreasing Pe, i.e., for an increasing influence of Brownian aggregation (due to a decrease in primary particle radius and, therefore, an increase in the diffusion coefficient) or an decrease in the hydrodynamic forces (due to a decrease in shear or an increase in primary particle radius), the value of the exponent n increases. This corresponds to a weaker dependency of the aggregation rate on the shear rate. For very small values of Pe the experimental values of the exponent n can be compared with a series expansion for the solution of the convection diffusion equation. The latter is presented by van de Ven[56] who gives the aggregation rate in the limit Pe $\rightarrow 0$ to be equal to the Brownian aggregation rate plus a term that is proportional to $\sqrt{G}$. This is in agreement with the measured exponent of $n = 0.5$ and it reflects the fact that for ever smaller value of Pe influence of G vanishes.

Conclusion

The aggregation kinetics of polystyrene latex particles with diameters equal to 120, 420, and 810 nm were investigated experimentally under turbulent conditions in a stirred tank. The broad range of particle sizes allowed us to investigate the transition from diffusion-controlled aggregation to purely shear-induced aggregation. Characterization of the time evolution of integral quantities of the cluster population, i.e., the root-mean-square radius of gyration, the zero-angle intensity of scattered light, and obscuration was done by small-angle static light scattering. It was found that for a given size of primary particles the time evolution of all integral quantities obtained at various stirring speeds, characterized by the volume average shear rate $\langle G \rangle$, can be scaled with a dimensionless time $\alpha_{exp} \times \langle G \rangle \times \phi \times t$. The prefactor α_{exp} represents an experimentally obtained aggregation efficiency which according to experimental data follows a power law of the form $\alpha_{exp} = \mathrm{Pe}^{-n}$ where Pe is the primary particle Péclet number. The exponent n is found to be inversely proportional to the primary particle size. Obtained values of the exponent n are in close agreement with data published in literature. Moreover, by varying the relative importance of Brownian motion with respect to shear significantly different evolutions of the measured integral quantities were observed. In half-logarithmic plots, the time evolution of $\langle R_g \rangle_n$ and $I(0)_n$ exhibit a concave shape for Pe $\ll 1$ and a convex shape for Pe $\gg 1$. According to our previous work[15] this can be explained by a variation of the shape of the CMD along the growth process due to varying contributions of Brownian motion and shear to the aggregation process.

Supporting Information

In Supporting Information the derivation of an analytical expression for the scaling exponent n, Eq. 9 plotted in Figure 5, is presented. It is based on an approximate expression for the rate of doublet formation under the influence of both Brownian and shear-induced aggregation derived by Zaccone et al.[62] This information is available free of charge via the Internet.

Acknowledgments

The authors thank Dr. Marco Lattuada, and Alessio Zaccone for the useful discussions and their helpful suggestions. This work was financially supported by the Swiss National Science Foundation (Grant No. 200020-113805/1).

Notation

Roman letters

A_H = Hamaker constant, J
c = correction factor for scaling of $I(0)$ with i, which is a function of d_p and d_f
$C_{ext}, C_{sca}, C_{abs}$ = extinction cross section, scattering cross section, absorption cross section, m^2
d_f = mass fractal dimension
d_p = primary particle diameter, nm
D = double diffusion coefficient, $D = k_B T/3\pi\eta r_p$, $m^2\ s^{-1}$
$G, \langle G \rangle$ = local shear rate, volume average shear rate $G = \sqrt{\varepsilon/\nu}$, s^{-1}
$I(0), I(0)_n$ = zero-angle intensity of scattered light, normalized zero-angle intensity, $I(0)_n = I(0)/I(0)_{t=0}$, au
$I(q)$ = intensity of scattered light, au
k = prefactor, which is assumed to be equal to unity for the particle sizes investigated
k_B = Boltzmann constant ($1.3806503 \times 10^{-23}$ $kg^2\ ms^{-2}\ K^{-1}$), $kg^2\ ms^{-2}\ K^{-1}$

K_{11} = rate of doublet formation, $m^3\ s^{-1}$
m = relative refractive index
M = ratio of moment ratios, $M = I(0)_n/\langle R_g\rangle_n$
n = refractive index, scaling exponent
N = number concentration, $N = \phi/V_p$, $1/m^3$
N_f = flow number, $N_f = A_H/\eta Gr^3$
Ob, Ob_n = obscuration, defined in Eq. 4, normalized obscuration $Ob_n = Ob/Ob_{t=0}$
Pe = Péclet number, defined in Eq. 1
$P(q)$ = form factor of primary particles
q = scattering vector amplitude, nm^{-1}
r,r_p = characteristic length scale (radius), primary particle radius, nm, μm
$\langle R_g\rangle$, $R_{g,p}$ = root-mean-square radius of gyration of the aggregate, $\langle R_g\rangle = \sqrt{\langle R_g^2\rangle}$, and the primary particles, μm
$\langle R_g\rangle_n$ = normalized root-mean-square radius of gyration, $\langle R_g\rangle_n = \langle R_g\rangle/R_{g,p}$
$S(q)$ = structure factor as a result of primary particle arrangement within the aggregate
t = time, s
T = absolute temperature (298K for room-temperature), K
V_p = primary particle volume, m^3

Greek letters

α_A,α_c,$\alpha_{doublet}$,α_{exp},$\alpha_{i,j}$ = aggregation efficiencies: from Moussa et al.[40] uniform, doublet, experimental ($\alpha_{exp} = Pe^{-n}$), and for aggregates of mass i and j
η = dynamic viscosity, 0.001 Pa s for water at 25°C, Pa s
θ = scattering angle, rad
λ,λ_L = laser wave length, London wavelength, nm
τ = turbidity, defined in Eq. 4, m^{-1}
τ_A = characteristic time of aggregation, s
τ_{exp},τ^*_{exp} = experimental dimensionless time, $\tau_{c,exp} = \alpha_{c,exp} \times \langle G\rangle \times \phi \times t$, and critical experimental dimensionless time
τ_s = dimensionless time of shear aggregation, $\tau_s = \langle G\rangle \times \phi \times t$
ϕ = solid-volume fraction

Abbreviations

CMD = cluster mass distribution
RDG = Rayleigh-Debye-Gans
rms = root-mean-square
SASLS = small-angle static light scattering

Literature Cited

1. Letterman RD, Amirtharajah A, O'Melia CR. *Coagulation and Flocculation*. In: *Water Quality and Treatment - A Handbook of Community Water Supplies*. 5th ed. Letterman RD, ed. McGraw-Hill; 1999: 6.1–6.66.
2. Odian G. *Principles of Polymerization* 4th ed. Hoboken, NJ: John Wiley & Sons, Inc.; 2004.
3. Lin MY, Lindsay HM, Weitz DA, Ball RC, Klein R, Meakin P. Universality in colloid aggregation. *Nature*. 1989;339:360–362.
4. Lin M, Lindsay HM, Weitz DA, Ball RC, Klein R, Meakin P. Universal diffusion-limited colloid aggregation. *J Phys: Condens Matter*. 1990;2:3093–3113.
5. Lin M, Lindsay HM, Weitz DA, Klein R, Ball RC, Meakin P. Universal reaction-limited aggregation. *Phys Rev A*. 1990;41:2005–2020.
6. Torres FE, Russel WB, Schowalter WR. Floc structure and growth-kinetics for rapid shear coagulation of polystyrene colloids. *J Colloid Interface Sci*. 1991;142:554–574.
7. Veerapaneni S, Wiesner MR. Hydrodynamics of fractal aggregates with radially varying permeability. *J Colloid Interface Sci*. 1996;177:45–57.
8. Kusters KA, Wijers JG, Thoenes D. Aggregation kinetics of small particles in agitated vessels. *Chemi Eng Sci*. 1997;52:107–121.
9. Brunk BK, Koch DL, Lion LW. Observation of coagulation in isotropic turbulence. *J Fluid Mech*. 1998;371:81–107.
10. Tontrup C, Gruy F, Cournil M. Turbulent aggregation of titania in water. *J Colloid Interface Sci*. 2000;229:511–525.
11. Gruy F. Formation of small silica aggregates by turbulent aggregation. *J Colloid Interface Sci*. 2001;237:28–39.
12. Selomulya C, Bushell G, Amal R, Waite TD. Aggregation mechanisms of latex of different particle sizes in a controlled shear environment. *Langmuir* 2002;18:1974–1984.
13. Waldner MH, Sefcik J, Soos M, Morbidelli M. Initial growth kinetics of aggregates in turbulent coagulator. *Powder Technol*. 2005;156:226–234.
14. Bäbler MU, Sefcik J, Morbidelli M, Baldyga J. Hydrodynamic interactions and orthokinetic collisions of porous aggregates in the Stokes regime. *Phys Fluids*. 2006;18:013302.
15. Soos M, Sefcik J, Morbidelli M. Master curves for aggregation and gelation: effects of cluster structure and polydispersity. *Ind Eng Chem Res*. 2007;46:1709–1720.
16. Bäbler MU, Moussa AS, Ehrl L, Soos L, Mazzotti M, Morbidelli M. Structure and kinetics of shear aggregation in turbulent flows. Early stage of aggregation. *AICHE J*. 2009; submitted
17. Bäbler MU. A collision efficiency model for flow induced coagulation of fractal aggregates. *AIChE J*. 2008;54:1748–1760.
18. Russel WB, Saville DA, Schowalter WR. *Colloidal Dispersion*. Cambridge: Cambridge University Press; 1999.
19. von Smoluchowski M. Versuch einer mathematischen Theorie der Koagulationskinetik kolloider Lösungen. *Zeitschrift für Physikalische Chemie*. 1917;92:129–168.
20. Camp TR, Stein PC. Velocity gradients and internal work in fluid motion. *J Boston Soc Civil Eng*. 1943;30:219–237.
21. Saffman PG, Turner JS. On the collision of drops in turbulent clouds. *J Fluid Mech*. 1956;1:16–30.
22. Birkner FB, Morgan JJ. Polymer flocculation kinetics of dilute colloidal suspensions. *J Am Water Works Assn*. 1968;60:175–191.
23. Higashitani K, Yamauchi K, Matsuno Y, Hosokawa G. Turbulent coagulation of particles dispersed in a viscous fluid. *J Chem Eng Jap*. 1983;16:299–304.
24. de Boer GBJ, Hoedemakers GFM, Thoenes D. Coagulation in turbulent flow: Part I. *Chem Eng Res Des*. 1989;67:301–307.
25. Kobayashi M, Maekita T, Adachi Y, Sasaki H. Colloid stability and coagulation rate of polystyrene latex particles in a turbulent flow. *Int J Miner Process*. 2004;73:177–181.
26. Li XY, Logan BE. Collision frequencies of fractal aggregates with small particles by differential sedimentation. *Environ Sci Technol*. 1997;31:1229–1236.
27. Li XY, Logan BE. Collision frequencies between fractal aggregates with small particles in a turbulently sheared fluid. *Environ Sci Technol*. 1997;31:1237–1242.
28. Spielman LA. Viscous interactions in brownian coagulation. *J Colloid Interface Sci*. 1970;33:562–571.
29. Honig EP, Roeberse GJ, Wiersema PH. Effect of hydrodynamic interaction on coagulation rate of hydrophobic colloids. *J Colloid Interface Sci*. 1971;36:97–109.
30. van de Ven TGM, Mason SG. Microrheology of colloidal dispersions. VII. Orthokinetic doublet formation of spheres. *Colloid Polymer Sci*. 1977;255:468–479.
31. Zeichner GR, Schowalter WR. Use of trajectory analysis to study stability of colloidal dispersion in flow fields. *AIChE J*. 1977;23: 243–254.
32. Zeichner GR, Schowalter WR. Effects of hydrodynamic and colloidal forces on the coagulation of dispersions. *J Colloid Interface Sci*. 1979;71:237–253.
33. Adler PM. Heterocoagulation in shear flow. *J Colloid Interface Sci*. 1981;83:106–115.
34. Adler PM. Interaction of unequal spheres I. Hydrodynamic interaction: Colloidal forces. *J Colloid Interface Sci*. 1981;84:461–474.
35. Higashitani K, Ogawa R, Hosokawa G, Matsuno Y. Kinetic-theory of shear coagulation for particles in a viscous-fluid. *J Chem Eng Jap*. 1982;15:299–304.
36. Brunk BK, Koch DL, Lion LW. Hydrodynamic pair diffusion in isotropic random velocity fields with application to turbulent coagulation. *Phys Fluids*. 1997;9:2670–2691.

37. Brunk BK, Koch DL, Lion LW. Turbulent coagulation of colloidal particles. *J Fluid Mech*. 1998;364:81–113.
38. Soos M, Moussa AS, Ehrl L, Sefcik J, Wu H, Morbidelli M. Effect of shear rate on aggregates size and morphology investigated under turbulent conditions in stirred tank. *J Colloid Interface Sci*. 2008;319:577–589.
39. Moussa AS, Ehrl L, Soos M, Lattuada M, Morbidelli M. Effect of pH on Flow-Induced Aggregation of Fully-Destabilized Polystyrene Latex. 2007 AIChE Annual Meeting, Salt Lake City, Utah, U, November 4–9, 2007.
40. Moussa AS, Soos M, Sefcik J, Morbidelli M. Effect of Solid volume fraction on aggregation and breakage in colloidal suspensions in batch and continuous stirred tank. *Langmuir*. 2007;23:1664–1673.
41. Ehrl L, Soos M, Morbidelli M. Dependence of aggregate strength, structure, and light scattering properties on primary particle size under turbulent conditions in stirred tank. *Langmuir* 2008;24:3070–3081.
42. Sorensen CM. Light scattering by fractal aggregates: A Review. *Aerosol Sci Technol*. 2001;35:648–687.
43. Kerker M. *The Scattering of Light and Other Electromagnetic Radiation*. New York: Academic Press: 1969.
44. Farias TL, Köylü ÖÜ, Carvalho MG. Range of validity of the Rayleigh-Debye-Gans theory for optics of fractal aggregates. *Applied Optics*. 1996;35:6560–6567.
45. Jones AR. Light scattering for particle characterization. *Prog Energy Combust Sci*. 1999;25:1–53.
46. Lambert S, Thill A, Ginestet P, Audic JM, Bottero JY. Structural interpretations of static light scattering patterns of fractal aggregates - I. Introduction of a mean optical index: Numerical simulations. *J Colloid Interface Sci*. 2000;228:379–385.
47. Tishkovets VP, Petrova EV, Jockers K. Optical properties of aggregate particles comparable in size to the wavelength. *J Quant Spectrosc Radiat Transfer*. 2004;86:241–265.
48. Petrova EV, Tishkovets VP, Jockers K. Polarization of light scattered by solar system bodies and the aggregate model of dust particles. *Solar Syst Res*. 2004;38:309–324.
49. Weiner BB. Particle and Droplet Sizing using Fraunhofer Diffraction. In: *Modern Methods of Particle Size Analysis*, Barth, H.G., ed. Hoboken, NJ; John Wiley & Sons, Inc: 1984; Vol. 73,135–172.
50. Soos M, Lattuada M, Sefcik J, Morbidelli M. Turbidity Spectra and Static Light Scattering in Mie Scattering Regime for Monitoring of Particle Formation Processes, International Congress on Particle Technology, PARTEC, Nuremberg, Germany, March 27–29, 2007.
51. Lattuada M, Ehrl L. Scattering properties of dense clusters of colloidal nanoparticles. *J Phys Chem B*. 2009;113:5938–5950.
52. Marchisio DL, Soos M, Sefcik J, Morbidelli M. Role of turbulent shear distribution in aggregation and breakage processes. *AIChE J*. 2006;52:158–173.
53. Marchisio DL, Soos M, Sefcik J, Morbidelli M, Barresi AA, Baldi G. Effect of fluid dynamics on particle size distribution in particulate processes. *Chem Eng Technol*. 2006;29:191–199.
54. Soos M, Wu H, Morbidelli M. A Taylor-Couette unit with lobed inner cylinder cross section. *AIChE J*. 2007;53:1109–1120.
55. Lattuada M, Wu H, Sandkühler P, Sefcik J, Morbidelli M. Modelling of aggregation kinetics of colloidal systems and its validation by light scattering measurements. *Chem Eng Sci*. 2004;59:1783–1793.
56. van de Ven TGM, Mason SG. Microrheology of colloidal dispersions. VIII. Effect of shear on peri-kinetic doublet formation. *Colloid Polym Sci*. 1977;255:794–804.
57. van de Ven TGM. Interactions between colloidal particles in simple shear-flow. *Adv Colloid Interface Sci*. 1982;17:105–127.
58. Selomulya C, Amal R, Bushell G, Waite TD. Evidence of shear-rate dependence on restructuring and breakup of latex aggregates. *J Colloid Interface Sci*. 2001;236:67–77.
59. Spicer PT, Pratsinis SE. Shear-induced flocculation: The evolution of floc structure and the shape of the size distribution at steady state. *Water Res*. 1996;30:1049–1056.
60. Prieve DC, Russel WB. Simplified predictions of Hamaker constants from Lifshitz theory. *J Colloid Interface Sci*. 1988;125:1–13.
61. Ackler HD, French RH, Chiang YM. Comparisons of Hamaker constants for ceramic systems with intervening vacuum or water: From force laws and physical properties. *J Colloid Interface Sci*. 1996;179:460–469.
62. Zaccone A, Wu H, Lattuada M, Morbidelli M. Charged molecular films on Brownian particles: Structure, interactions, and relation to stability. *J Phys Chem B*. 2008;112:6793–6802.
63. Lattuada M, Morbidelli M. Generalized model for the aggregation rate of colloidal nanoparticles and clusters induced by shear in the presence of repulsive interactions, 12th The Nanotechnology Conference and Trade Show, NIST Nanotech, Boston; 2008.

Manuscript received Oct. 10, 2008, and revision received Mar. 13, 2009.